Post-Print

This is the accepted version of:

G. Cammi, C.C. Conti, A. Spinelli, A. Guardone
Experimental Characterization of Nozzle Flow Expansions of Siloxane MM for ORC Turbines Applications
Energy, Vol. 218, 2021, 119249 (12 pages)
doi:10.1016/j.energy.2020.119249

The final publication is available at https://doi.org/10.1016/j.energy.2020.119249

Access to the published version may require subscription.

Experimental characterization of nozzle flow expansions of siloxane MM for ORC turbines applications

Giorgia Cammi[a], Camilla Cecilia Conti[b], Andrea Spinelli[a,*], Alberto Guardone[b]

[a] *Politecnico di Milano, Energy Department, via Lambruschini 4, 20156, Milano, Italy*
[b] *Politecnico di Milano, Aerospace Science and Tecnology Department, via La Masa 34, 20156, Milano, Italy*

Abstract

This paper reports extensive experimental results characterizing the supersonic expansion of organic vapor MM (hexamethyldisiloxane, $C_6H_{18}OSi_2$) in conditions representative of actual Organic Rankine Cycle (ORC) turbine operations, in the close proximity of the liquid-vapor saturation curve. Experiments were conducted on the Test Rig for Organic VApors (TROVA), at the Laboratory of Compressible fluid-dynamics for Renewable Energy Applications (CREA Lab) of Politecnico di Milano. A planar nozzle was tested, featuring a design exit Mach number of 1.6. Nozzle flow expansions were characterized by measuring total pressure, total temperature, static pressures along the nozzle axis and by performing schlieren visualizations. It was verified that the expansion is influenced by total inlet conditions due to the non-ideal nature of the flow. Data on nozzle flow expansions with total conditions having compressibility factor Z_T ranging from 0.39 (strongly non-ideal) to 0.98 (almost ideal) was gathered. The difference between pressure ratio measured at the lowest Z_T was higher by 10%-20% with respect to the one measured at the highest Z_T in all axial locations analyzed.

A very large experimental dataset was analyzed to assess the influence of both the total compressibility factor and of the total fundamental derivative of gas-

*Corresponding author
Email address: andrea.spinelli@polimi.it

dynamics on the non-dimensional pressure distribution along the nozzle axis. It was investigated whether one between parameters Z_T and Γ_T could be used to univocally identify a non-dimensional nozzle expansion.
The present experimental investigation provides significant validation data for the improvement of CFD simulation codes and of design tools for siloxane fluids in general and for siloxane MM in particular.

Keywords: Experiments in non-ideal compressible flows, Non-ideal supersonic expanding flows, Siloxane MM, Test Rig for Organic Vapors TROVA, nozzle expansion, ORC power systems.

---

1. Introduction

Organic Rankine Cycle (ORC) power systems are a convenient option for power production in the 0.1 to 100 MW range when low/medium source temperatures are involved, thanks to their relatively high efficiency, low cost and plant simplicity with respect to traditional steam Rankine cycles. Such temperatures and power ranges are often found in the case of renewable energy sources, such as geothermal reservoirs, biomass combustion and waste heat recovery from several industrial processes (power plants, cement and glass factories) ([1, 2, 3]).
ORCs involve flows of heavy and complex organic compounds in thermodynamic regions close to the liquid-vapor saturation curve and to the critical point, where intermolecular forces are not negligible. As a result, ORC turbine flows differ from standard turbomachinery ones because they are highly supersonic and show significant non-ideal gas effects, such as flow field dependence on stagnation conditions ([4, 5, 6]). Given this, the design of such machines is particularly critical, also considering that turbine efficiency impacts the economic competitiveness of the ORC technology. Current computational tools are based on advanced CFD codes ([7, 8, 9, 10, 11]) embedding state-of-the-art thermodynamic models ([12, 13]), but experimental data are only recently becoming available in literature for comparison and verification ([14, 4, 5, 15]). This is mainly due to the peculiar features of organic fluid flows, as the high temperature, the vicinity

to the saturation curve and to the thermal stability limits, which challenge the success of ad-hoc experimental campaigns. Nevertheless, several experimental facilities were recently constructed, such as the FAST ([16]) and the ORCHID ([17]) at TU Delft, the CLOWT ([18]) at Muenster University of Applied Sciences, the Imperial College Dense Gas Blowdown Facility ([15]), and the Test Rig for Organic VApors (TROVA) [19] at the Laboratory of Compressible fluid-dynamics for Renewable Energy Applications (CREA Lab) of Politecnico di Milano.

The experimental campaigns presented in this paper were conducted on the TROVA facility. It is a blow-down wind tunnel specifically designed to reproduce supersonic flows of organic vapors in conditions representative of ORC turbine expansions. The TROVA test section can be equipped with planar nozzles, designed for different fluids and/or operating conditions, and it can also accommodate linear blade cascades. In the present experimental campaign, a planar nozzle was tested with siloxane fluid MM (hexamethyldisiloxane, $C_6H_{18}OSi_2$), yielding a design exit Mach number of 1.6 (a typical value for ORC turbine vanes, especially for initial stages).

Nozzle expansions were characterized by total temperature and total pressure measures, by static pressure measurements along the axis and by the Schlieren technique to visualize the two-dimensional density gradient field along the axis direction. A wide range of inlet conditions was explored in order to systematically span the thermodynamic region of superheated vapor. Conditions varied from highly non-ideal to almost ideal gas conditions, with a compressibility factor evaluated at total conditions ranging between 0.39 and 0.98.

Results allowed to verify that nozzle expansion is influenced by total inlet conditions because of the non-ideal nature of the flow. Total inlet conditions are identified measuring total temperature T_T and total pressure P_T. These two parameters univocally identify a supersonic expansion inside a nozzle with a given geometry.

However, it was investigated whether a single parameter can be used to assess the level of non-ideality of a nozzle flow and thus, to characterize the expan-

sion and predict pressure ratio profiles with acceptable accuracy. Analyzed parameters were the compressibility factor Z_T and the fundamental derivative of gas-dynamics Γ_T, both evaluated at total conditions (subscript $'T'$). Z_T is defined in Equation 1, where R is the gas constant and $\rho_T = \rho(T_T, P_T)$ is the stagnation density:

$$Z_T = \frac{P_T}{T_T R \rho(T_T, P_T)} \tag{1}$$

The compressibility factor Z identifies how much the volumetric behaviour of a fluid differs from that of an ideal gas. Thus, it can be used to quantify the level of flow non-ideality. The fundamental derivative of gasdynamics instead provides information about admissible nozzle flow behaviors since it represents the non-dimensional variation of the speed of sound with pressure along an isentropic process. At total conditions, it is defined in Equation 2 where c is the speed of sound, v is the specific volume:

$$\Gamma_T = \frac{c_T^4}{2v_T^3}\left[\left(\frac{\partial^2 v}{\partial P^2}\right)_s\right]_T = 1 + \frac{c_T}{v_T}\left[\left(\frac{\partial c}{\partial P}\right)_s\right]_T \tag{2}$$

A Helmoltz energy based fundamental relation of Span-Wagner type was used to calculate all derived thermodynamic quantities [13].

The paper is structured as follows. Section 2 describes the facility, the implemented measurement techniques and the selected test conditions. Results showing non-ideal gas effects are presented in Section 3, while the influence of the total compressibility factor and of the total fundamental derivative of gasdynamics are analyzed in Section 4. A comparison between Z_T and Γ_T perfomances in predicting non-dimensional nozzle expansions of siloxane MM is also included here. Section 5 extends the conclusions, drawn for fluid MM in the thermodynamic region explored with experiments, to a wider region and to other fluids of interest for ORC applications with the use of quasi-1D nozzle theory. Section 6 finally draws the conclusions of this work.

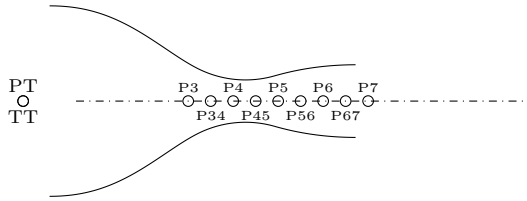

Figure 1: Nozzle M1.6: sketch of the nozzle profile with position of measurement points.

2. Experimental set-up

2.1. The Test-Rig for Organic VApors (TROVA)

The Test-Rig for Organic VApors (TROVA) is a blow-down wind tunnel specifically designed to reproduce flows of non-ideal vapors in conditions representative of ORC turbines expansions. The working fluid is isochorically heated in a High Pressure Vessel (HPV) until the desired temperature and pressure conditions are reached. Vapor is discharged at the opening of the Main Control Valve (MCV) from the HPV to a Low Pressure Vessel (LPV) by passing through a settling chamber (plenum) and the test section, in which it is expanded from subsonic to supersonic velocity through a planar converging-diverging nozzle. The vapor is condensed in the LPV and pumped back to the HPV by means of a membrane pump. More details on the design and operation of the TROVA can be found in [19, 20].

2.2. Test Section

The TROVA test section is planar and can accommodate straight-axis nozzles with a rectangular cross-section, designed for the considered fluid and operating conditions according to the procedure described in [21]. The straight-axis geometry allows to characterize the flow field at underexpanded nozzle regimes by using the isentropic flow hypothesis, thus avoiding the need for calibrated pressure probes, which are currently not available for organic vapors flows.

The tested nozzle is named $M1.6$ (Fig. 1) since it was designed for siloxane fluid MM to produce a uniform exit flow with Mach number $M = 1.6$, with $P_T = 21.4\ bar$ and $T_T = 254°C$. It is characterized by a throat semi-height of $H = 8\ mm$ and by a non-dimensional curvature at the throat, identified by the ratio between the radius of the circular arc shaping the throat region and the throat semi-height, of $r_t = 5$.

2.3. Measurements Setup and Instrumentation

Sixteen pressure taps of 0.3 mm in diameter are machined onto the rear steel plate along the nozzle axis. Each tap is connected to a pressure transducer through a $\approx$ 50 mm long line, providing a measure of the wall static pressure. Not all taps are simultaneously active during a single test. Nozzle total pressure P_T and temperature T_T are measured in the plenum upstream the test section, where flow velocity is low enough (about 1 m/s) for kinetic energy to be negligible. Thus, P_T is measured with a wall pressure transducer and T_T with the use of two thermocouples, one of K-type (hot junction of 0.15 mm diameter) and one of J-type (hot junction of 0.25 mm diameter). Pressure transducers are of piezo-resistive type. Due to their temperature sensitivity, they were calibrated both in pressure and temperature from 1 bar to full scale (3.5 bar $\leq$ FS $\leq$ 40 bar) and from 25°C to 300°C. Thermocouples were calibrated in the same temperature range (25° - 300°C). The expanded uncertainty is of the order of 0.07 % of the full scale for pressure sensors and of about 1°C for thermocouples. Data sampling frequency for temperature and pressure measurements is 1 kHz. Further details on instrumentation can be found in [4].

2.4. Test Description and Conditions

Each test starts as the MCV is opened and flow is discharged through the nozzle. Test time is about 140 s, excluding the valve opening transient (about 2 s). Tests end as the nozzle reaches over-expanded conditions with shocks waves entering in the nozzle. Since no control on total pressure is operated, P_T

and T_T decrease in time as the HPV empties and a wide range of thermodynamic states are explored during a single test run, from initial strong non-ideal conditions to the ideal gas state. Nozzle relaxation time is more than two orders of magnitude lower than the emptying time of the HPV ([19]), so that the nozzle flow can be assumed in a steady state at each sampled instant. To illustrate this, Figure 2a reports several selected total conditions, all belonging to the same test. As the test proceeds, going from condition a to condition h, total pressure and temperature decrease. Consequently the total compressibility factor, defined in Equation 1 increases towards unity during the test as dilute conditions are approached. Each total condition reported in Figure 2a refers to the corresponding isentropic expansions plotted in Figure 2b.

Several tests were performed and flows characterized by the same total conditions were reported in different tests. Comparison of this data proved consistency and repeatability of the performed measurements. This comparison is not reported here for brevity.

Among all tests carried out during the experimental campaign, seven were selected to be analyzed in the present paper: tests 21MM, 28MM, 30MM, 31MM, 33MM, 40MM, 43MM and 44MM. They are summarized in Table 1, which also reports the most and the least non-ideal total conditions reached in each tests.

3. Experimental evidence of non-ideal compressible fluid effects

Test 44MM achieved the highest pressures and temperatures of the whole experimental campaign. Nozzle expansions characterized by total compressibility factors, ranging from $Z_T^{min} = 0.45$ to $Z_T^{max} = 0.85$ were extracted from this test. Figure 2a reports the total conditions at which data were analysed on a $P - T$ diagram with Z contours, with points labeled from c to k at increasing values of Z_T, thus levels of ideality. Figure 2b shows the corresponding isentropic expansions on a $T - s$ diagram.

Pressure ratio measured along the nozzle axis during these expansions can be

Test ID	Nozzle	Most non-ideal condition			Least non-ideal condition		
		P_T $[bar]$	T_T $[^\circ C]$	Z_T	P_T $[bar]$	T_T $[^\circ C]$	Z_T
21MM	*M1.6*	10.576	222.1	0.71	0.840	215.5	0.98
28MM	*M1.6*	8.367	200.8	0.74	0.731	204.4	0.98
30MM	*M1.6*	7.796	206.8	0.77	0.570	202.9	0.99
31MM	*M1.6*	6.266	185.3	0.78	0.654	193.5	0.98
33MM	*M1.6*	12.290	234.5	0.69	1.605	221.7	0.96
40MM	*M1.6*	18.971	259.4	0.57	2.632	234.5	0.95
43MM	*M1.6*	23.54	262.4	0.39	5.850	232.6	0.87
44MM	*M1.6*	23.93	266.7	0.43	5.710	236.6	0.88

Table 1: Tests selected for analysis in the present paper

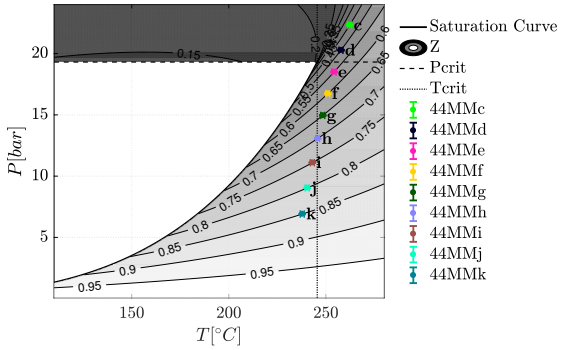

(a) *Total conditions for MM reported on a $P-T$ diagram with Z contour, saturation curve (black line), critical pressure and critical temperature (dotted black lines).*

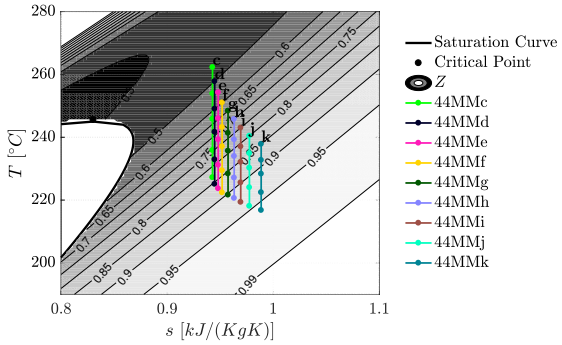

(b) *Isentropic nozzle expansions plotted on a $T-s$ diagram with the saturation curve (black line). Dots along each expansion correspond to temperatures computed using the static pressure measured along the axis.*

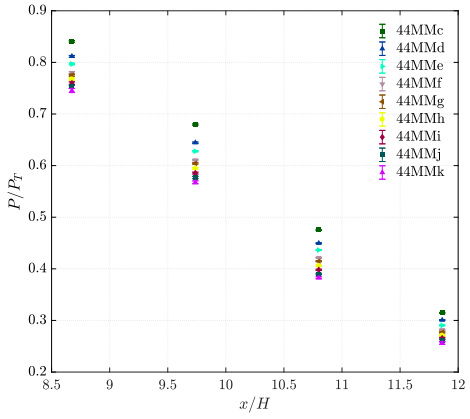

(c) *P/P_T trends along the nozzle axis extracted from test 44MM.*

Figure 2: Analysis of different flows extracted from test *44*.

used to prove the influence of non-ideal fluid effects. Indeed, following *quasi-1D* theory, if the ideal gas equation of state is applicable, pressure ratios along the nozzle axis are independent of total conditions. Thus, the pressure ratio change with total conditions can be ascribed to non-ideal compressible fluid effects [6]. Figure 2c shows pressure ratio trends along the nozzle axis during test 44MM. Pressure ratios decrease going from the most non-ideal condition 44MMc, characterized by $Z_T^{min} = 0.45$, to the most ideal one 44MMk, featuring $Z_T^{max} = 0.85$ much closer to the ideal gas limit of 1. At the axial location $x/H = 9.74$, located just downstream the geometrical throat, the pressure ratio at Z_T^{min} is 1.2 times the one at Z_T^{max}. In general, in all axial locations where pressure measurements are available, the difference between the pressure ratio measured at the highest P_T and T_T is higher by 10%-20% with respect to the one measured at the lowest P_T and T_T. This discrepancy is one order of magnitude higher than measurement uncertainty, thus it can only be ascribed to non-ideal compressible fluid effects.

These findings are consistent with the behaviour predicted by the *quasi-1D* nozzle theory, as reported in Section 5, and was experimentally observed also during previous experimental campaigns with fluid siloxane MDM, as described in [4].

4. Analysis of the nozzle flow expansion

Results presented in Section 3 prove the dependence of pressure ratio profiles on the total conditions at which the nozzle is operated, univocally characterized by total pressure P_T and total temperature T_T. However, if coupled with a suitable thermodynamic model ([13]), P_T and T_T can be used to compute both the total compressibility factor Z_T and the total fundamental derivative of gasdynamics Γ_T, as defined in Equations 1 and 2 respectively.

The compressibility factor can be used as a non-dimensional parameter to characterize the volumetric behavior of a non-ideal gas at a specific thermodynamic point. Since it identifies how much volumetric behavior differs from that of an ideal gas, it can be used to quantify the level of flow non ideality.

The value of the fundamental derivative of gasdynamics Γ, instead, provides information about the admissible flow behaviors. Indeed, the fundamental derivative of gasdynamics can be interpreted as the non-dimensional measure of the variation of speed of sound with pressure along an isentropic process. A thermodynamic region exhibiting $\Gamma < 1$ can be found only in fluids characterized by a high molecular complexity. Flows characterised by $\Gamma < 1$ are significantly different from ideal-gas ones since some peculiar behaviors are admissible [22]. Indeed, in this case, speed of sound c increases along expansions, possibly leading to a decrease of the local Mach number [23]. Moreover, phenomena such as the discontinuous increase of Mach number across oblique shocks become possible.

Since both quantities Z_T and Γ_T influence nozzle flow behavior, it was investigated whether one of them alone could be used to univocally identify a non-dimensional nozzle expansion. Thus, the aim is to investigate whether they can be used to predict pressure ratio profiles by resorting to one parameter only instead of the both P_T and T_T.

4.1. Influence of total compressibility factor Z_T

Sets of different expansions sharing the same Z_T but featuring different P_T and T_T were chosen in order to investigate whether parameter Z_T is sufficient to assess the level of non-ideality of a nozzle flow and thus, to characterize the non-dimensional flow field in terms of pressure ratios.

Figure 3 reports total conditions of selected nozzle flows. Expansions sharing the same Z_T are marked with the same letter, from letter a corresponding to $Z_T = 0.39$ to letter n indicating $Z_T = 0.98$. Comparisons between pressure ratio profiles of different tests at different total conditions and same Z_T are reported in Figure 4. Detailed results are presented for $Z_T = 0.45$ (corresponding to label c), $Z_T = 0.50$ (label d), $Z_T = 0.70$ (label h), $Z_T = 0.80$ (label j), $Z_T = 0.90$ (label l) and $Z_T = 0.98$ (label n).

It can be noticed that an appreciable difference between pressure ratio profiles is present only at $Z_T = 0.45$ (Fig. 4a) and $Z_T = 0.50$ (Fig. 4b). Profiles are

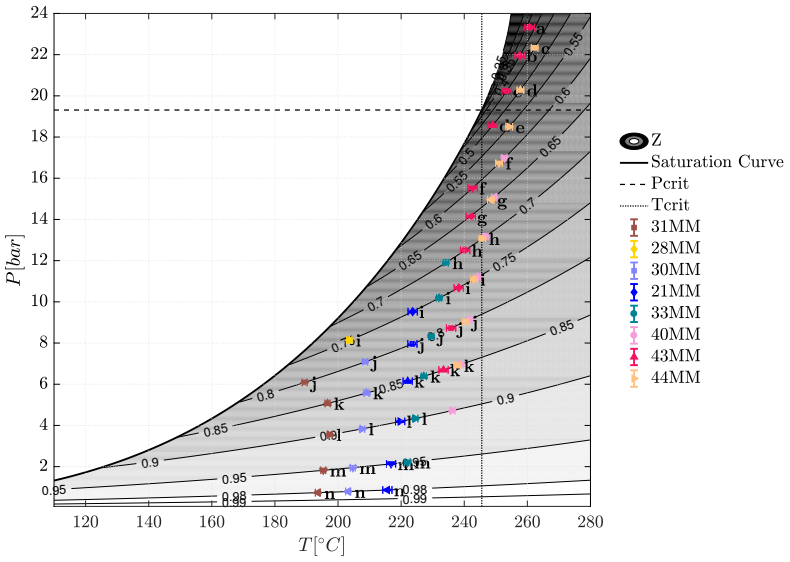

Figure 3: $P-T$ diagram with Z contour reporting the total conditions characterizing all the expansions analyzed to assess the influence of Z_T on pressure ratio profiles. The colors identify all expansions extracted from a single test.

almost superimposed in all other figures.

It is possible to quantify the discrepancy between pressure ratio profiles of expansions having different total pressure and temperature but sharing the same Z_T through the percentage difference $\Delta_{\Pi}^{Z_T}\%$ defined as:

$$\Delta_{\Pi}^{Z_T}\% = \frac{max\left[\Pi(Z_T)\right] - min\left[\Pi(Z_T)\right]}{min\left[\Pi(Z_T)\right]} \cdot 100 \tag{3}$$

where $max\left[\Pi(Z_T)\right]$ and $min\left[\Pi(Z_T)\right]$ refer to the maximum and the minimum values of pressure ratio registered in a specific axial location among all expansions sharing the same Z_T.

The percentage difference $\Delta_{\Pi}^{Z_T}\%$ is plotted in figures 5b, 5d, 5f. It can be noticed that going from $Z_T = 0.45$ towards more dilute conditions at higher Z_T, $\Delta_{\Pi}^{Z_T}\%$ decreases, consistently with a lower influence of total conditions as the ideal gas limit is approached.

Considering their importance in describing flow non-ideality and admissible behaviour, profiles of local Z and Γ along expansions are analyzed in Figures 5a,

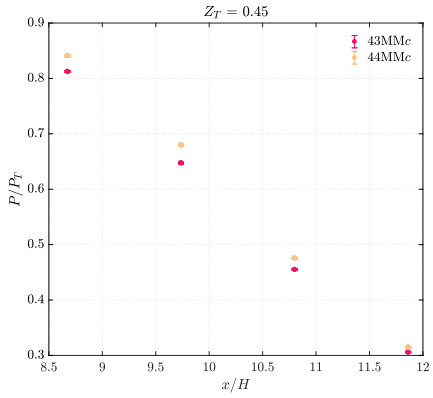

(a) $Z_T = 0.45$.

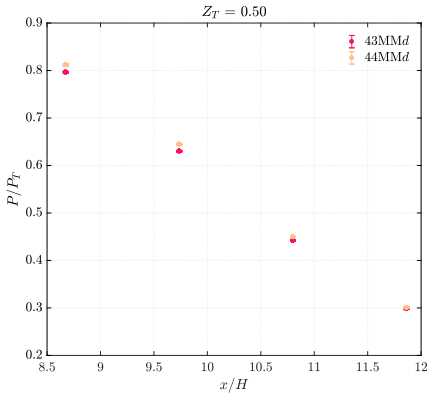

(b) $Z_T = 0.50$.

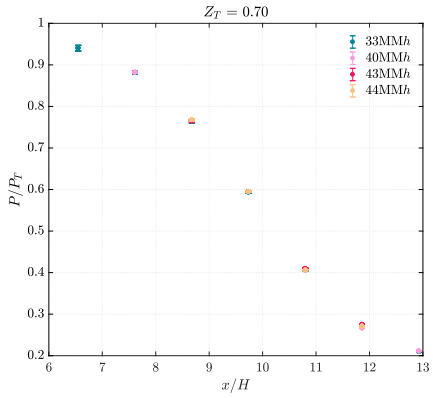

(c) $Z_T = 0.70$.

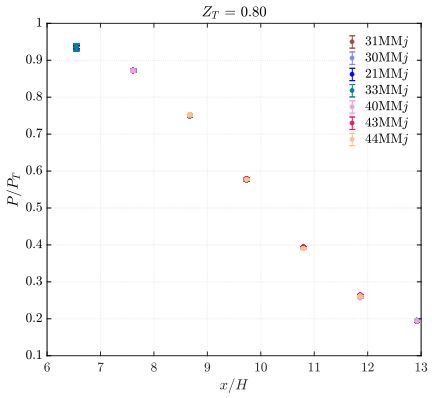

(d) $Z_T = 0.80$.

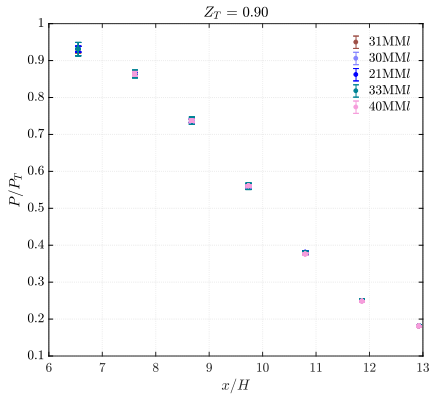

(e) $Z_T = 0.90$.

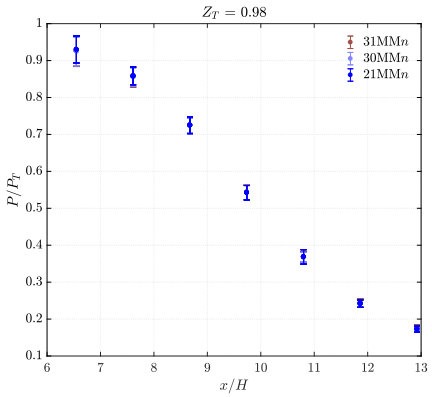

(f) $Z_T = 0.98$.

Figure 4: Pressure ratio profiles along the nozzle axis for all different total conditions sharing *(a)* $Z_T = 0.45$, *(b)* $Z_T = 0.50$, *(c)* $Z_T = 0.70$, *(d)* $Z_T = 0.80$, *(e)* $Z_T = 0.90$, *(f)* $Z_T = 0.98$.

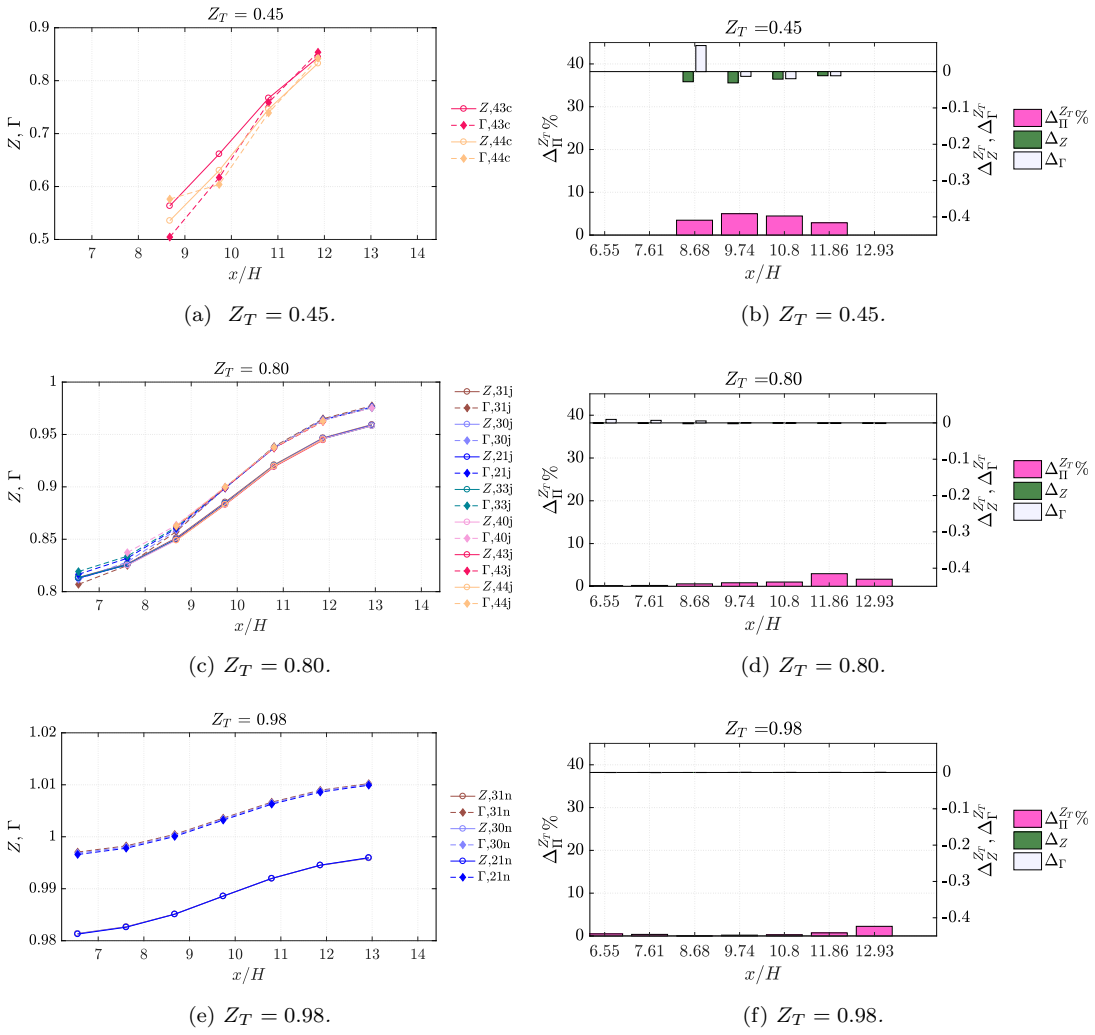

(a) $Z_T = 0.45$. (b) $Z_T = 0.45$.

(c) $Z_T = 0.80$. (d) $Z_T = 0.80$.

(e) $Z_T = 0.98$. (f) $Z_T = 0.98$.

Figure 5: On the left side: Z and Γ profiles on the nozzle axis of different expansions sharing *(a)* $Z_T = 0.45$, *(d)* $Z_T = 0.80$, *(f)* $Z_T = 0.98$. Profiles were computed from the static pressure measurements as $Z(P, s)$ and $\Gamma(P, s)$. On the right side: the left axis reports in pink bars the percentage difference $\Delta_\Pi^{Z_T}\%$ (Eq. (3)) between pressure ratios. The right axis reports in green bars the differences between compressibility factors $\Delta_Z^{Z_T}$ (Eq. (4)) and in gray bars the differences between the fundamental derivative of gas-dynamics $\Delta_\Gamma^{Z_T}$ (Eq. (5)).

5c, 5e. These quantities are computed from measured T_T, P_T and P by resorting to the isentropic flow hypothesis. In principle, starting from the same value of Z_T does not necessarily result in the same Z profiles. Indeed, deviations in the Z profiles tend to increase approaching the critical point where the Z gradients along isentropes are higher. However, experiments show that profiles are superimposed for all expansions sharing $Z_T \geq 0.60$. It can also be noticed that Γ profiles are almost superimposed for all conditions sharing $Z_T \geq 0.60$, while they considerably differ in the first axial locations in Figures 5a for $Z_T = 0.45$. It is possible to quantify the discrepancies between different Z and Γ profiles sharing the same Z_T through quantities $\Delta_Z^{Z_T}$ (Eq. (4)) and $\Delta_\Gamma^{Z_T}$ (Eq. (5)) defined in a similar way to $\Delta_\Pi^{Z_T}\%$ as:

$$\Delta_Z^{Z_T} = Z_{max[\Pi(Z_T)]} - Z_{min[\Pi(Z_T)]} \tag{4}$$

$$\Delta_\Gamma^{Z_T} = \Gamma_{max[\Pi(Z_T)]} - \Gamma_{min[\Pi(Z_T)]} \tag{5}$$

These quantities are plotted in Figures 5b, 5d, 5f, where it can be noticed that they are always well below 0.05.

It can be concluded that, in the thermodynamic region explored between $Z_T = 0.60$ to $Z_T = 0.98$, parameter Z_T can be used as univocal identifier of non-dimensional MM nozzle expansions in a given geometry. Contrarily, in the region where $Z_T < 0.60$ another parameter is needed to univocally characterize a non-dimensional nozzle flow. The following section investigates whether Γ_T is a better parameter than Z_T for nozzle flow characterization and if it can complement the latter in thermodynamic regions where $Z_T < 0.60$.

4.2. Influence of total fundamental derivative of gasdynamic Γ_T

First of all, an analysis similar to the one presented in the previous section was carried out to assess the influence of Γ_T on the nozzle flow expansion. Several expansions sharing the same Γ_T but having different total conditions (P_T, T_T) were compared, as reported in Figure 6 on a $P - T$ diagram with a contour of Γ. All expansions sharing the same Γ_T are marked with the same letter, from letter m for $\Gamma_T = 0.55$ to letter z for $\Gamma_T = 0.99$.

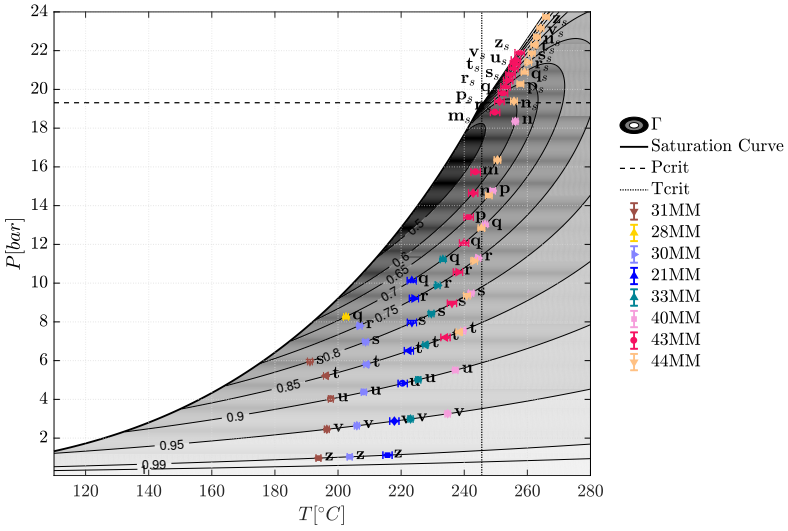

Figure 6: $P-T$ diagram with Γ contour reporting total conditions characterizing expansions analyzed to assess the influence of the total fundamental derivative of gas-dynamics Γ_T on pressure ratio profiles. The colors identify all expansions extracted from a single test.

Comparisons between pressure ratio profiles of different tests at different total conditions and same Γ_T are reported in Figure 7. The values of Γ_T selected for analysis here are: $\Gamma_T = 0.60$ (corresponding to label n), $\Gamma_T = 0.70$ (label q), $\Gamma_T = 0.75$ (label r), $\Gamma_T = 0.80$ (label s for all tests), $\Gamma_T = 0.90$ (label u) and $\Gamma_T = 0.99$ (label z). It can be noticed that pressure ratio profiles exhibit higher deviations than what was observed comparing profiles sharing the same Z_T (Section 4.1). In particular, all profiles marked with the subscript s are higher than the others.

The s subscript identifies expansions starting from supercritical conditions and occuring close to the critical point. Indeed, near the critical point, Γ isolines form a 'closed' region since they exhibit a higher gradient which also changes sign (from positive to negative). Thus, in a small thermodynamic region, the value of Γ_T spans from very low values to values larger than one. These same latter values also characterize thermodynamic regions featuring much more rar-

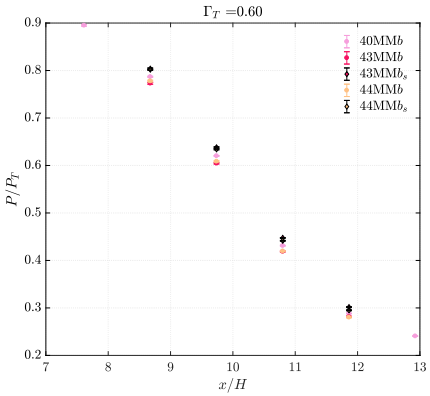

(a) $\Gamma_T = 0.60$.

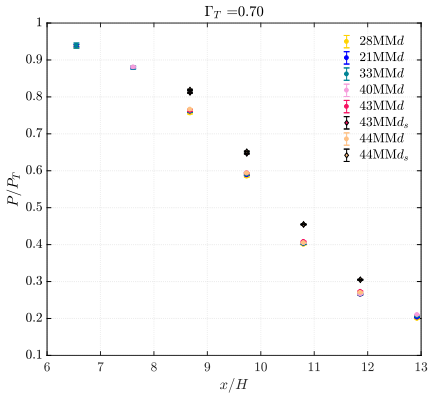

(b) $\Gamma_T = 0.70$.

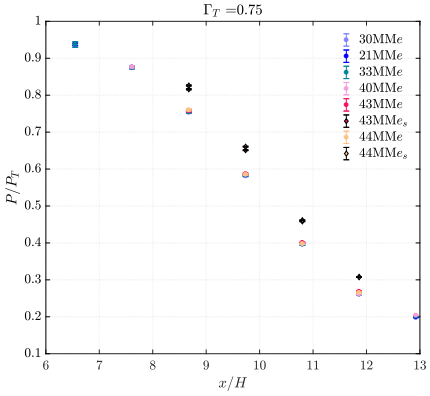

(c) $\Gamma_T = 0.75$.

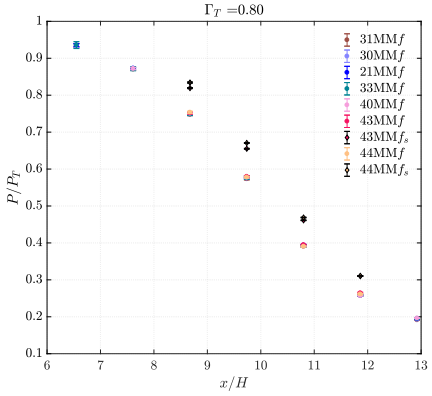

(d) $\Gamma_T = 0.80$.

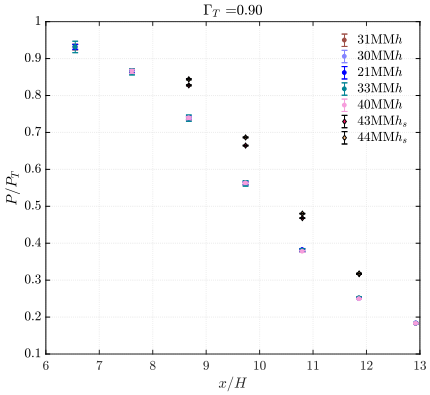

(e) $\Gamma_T = 0.90$.

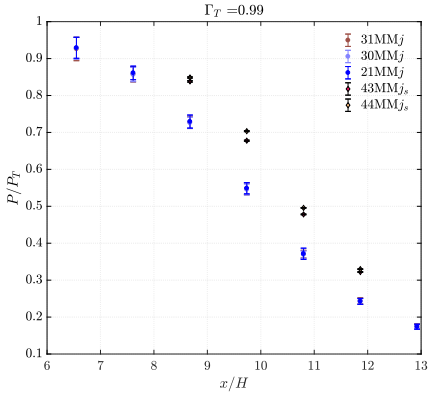

(f) $\Gamma_T = 0.99$.

Figure 7: Pressure ratio profiles along the nozzle axis for all different total conditions sharing *(a)* $\Gamma_T = 0.60$, *(b)* $\Gamma_T = 0.70$, *(c)* $\Gamma_T = 0.75$, *(d)* $\Gamma_T = 0.80$, *(e)* $\Gamma_T = 0.90$, *(f)* $\Gamma_T = 0.99$.

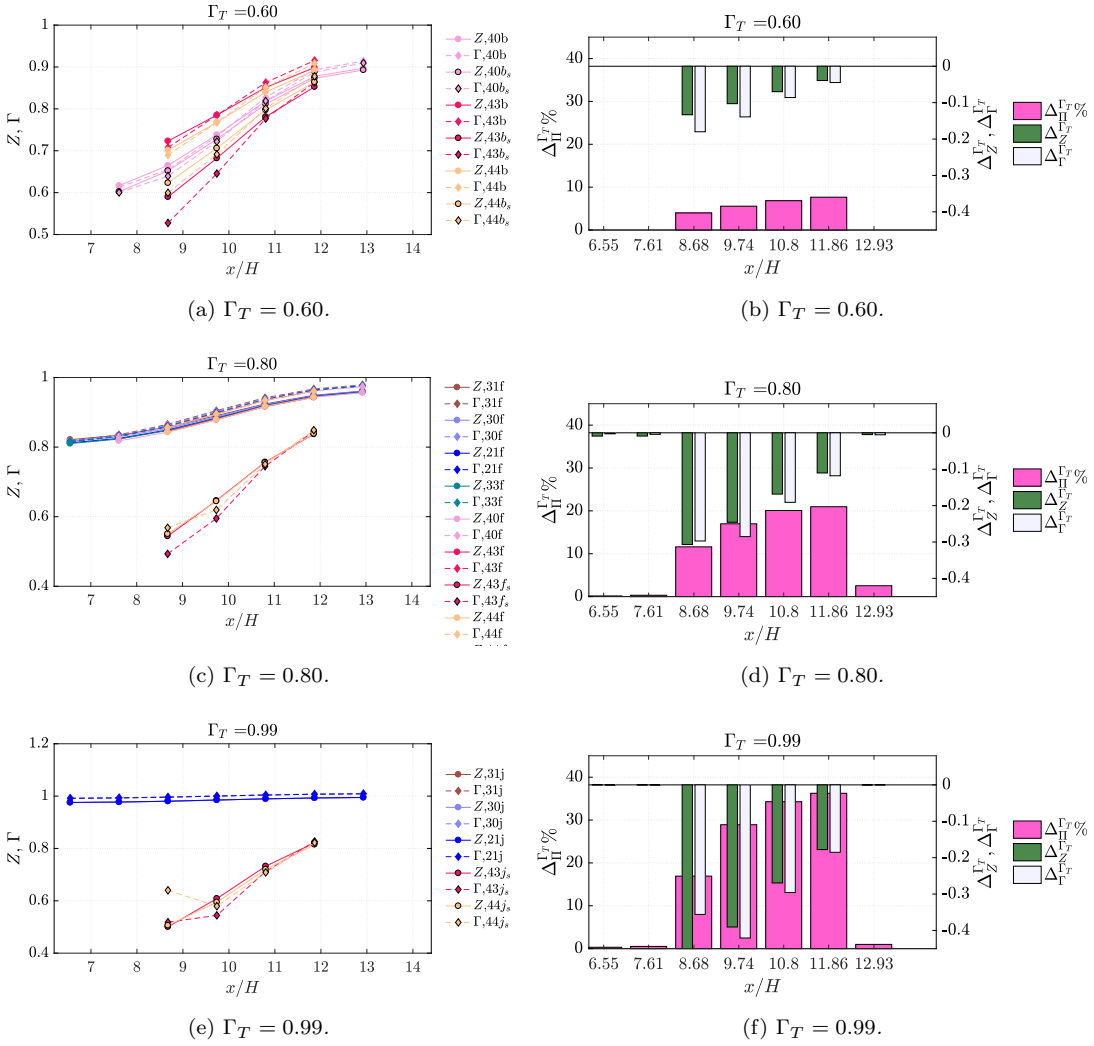

(a) $\Gamma_T = 0.60$.

(b) $\Gamma_T = 0.60$.

(c) $\Gamma_T = 0.80$.

(d) $\Gamma_T = 0.80$.

(e) $\Gamma_T = 0.99$.

(f) $\Gamma_T = 0.99$.

Figure 8: Left side: Z and Γ profiles on the nozzle axis of different expansions sharing *(a)* $\Gamma_T = 0.60$, *(d)* $\Gamma_T = 0.80$, *(f)* $\Gamma_T = 0.99$. The profiles were computed from the static pressure measurements as $Z(P, s)$ and $\Gamma(P, s)$. Right side: The left axis shows in pink bars the percentage difference $\Delta_\Pi^{\overline{\Gamma_T}}\%$ (Eq. (6)) between pressure ratio. The right axis reports in green bars the differences between compressibility factors $\Delta_Z^{\overline{\Gamma_T}}$ (Eq. (7)) and in gray bars the differences between the fundamantal derivative of gas-dynamic $\Delta_\Gamma^{\overline{\Gamma_T}}$ (Eq. (8)).

efied conditions. Indeed, as Γ_T increases, expansions starting from supercritical conditions depart more significantly from the ones sharing the same Γ_T but having much lower P_T and these result in big discrepancies in the pressure ratio profiles. These can again be quantified by resorting to the percentage difference $\Delta_{\Pi}^{\Gamma_T}\%$ defined as:

$$\Delta_{\Pi}^{\Gamma_T}\% = \frac{max\left[\Pi(\Gamma_T)\right] - min\left[\Pi(\Gamma_T)\right]}{min\left[\Pi(\Gamma_T)\right]} \cdot 100 \tag{6}$$

where $max\left[\Pi(\Gamma_T)\right]$ and $min\left[\Pi(\Gamma_T)\right]$ refer to the maximum and minimum value of pressure ratio registered in a specific axial location among all the expansions sharing same Γ_T.

This quantity is plotted in Figures 8b, 8d and 8f, where it can be noticed that at increasing Γ_T, the value of $\Delta_{\Pi}^{\Gamma_T}\%$ increases in all axial locations where pressure measurements are available also at supercritical conditions. Indeed, unfortunately, it was possible to measure static pressures during the tests reaching supercritical conditions only between $x/H = 8.68$ and $x/H = 11.86$.

The profiles of Γ and Z, calculated from the static pressure measured along the nozzle axis, show a situation similar to pressure ratio profiles. They are reported in figures 8a, 8c and 8c where it can be noticed that profiles marked with the subscript s are markedly lower than the others. Indeed, the values of $\Delta_Z^{\Gamma_T}$ and $\Delta_{\Gamma}^{\Gamma_T}$ are much higher than the ones of $\Delta_Z^{Z_T}$ and $\Delta_{\Gamma}^{Z_T}$ found during the previous analysis. Discrepancies are reported in figures 8b, 8d and 8f and reach values as high as 0.4. Moreover, they increase towards higher values of Γ_T.

$$\Delta_Z^{\Gamma_T} = Z_{max[\Pi(\Gamma_T)]} - Z_{min[\Pi(\Gamma_T)]} \tag{7}$$

$$\Delta_{\Gamma}^{\Gamma_T} = \Gamma_{max[\Pi(\Gamma_T)]} - \Gamma_{min[\Pi(\Gamma_T)]} \tag{8}$$

It can be concluded that quantity Γ_T alone cannot be used to identify the level of non-ideality of a nozzle flow of siloxane MM. Indeed, the same values of Γ_T are found in thermodynamic regions featuring rarefied conditions, where non-ideal compressible effects are negligible, and also in regions close to the critical point where non-ideal effects play a major role.

Nevertheless, parameter Γ_T can be coupled with Z_T to univocally identify a non-dimensional MM nozzle flow in regions where Z_T alone is not sufficient. Indeed, in the thermodynamic region of interest for ORC applications with fluid MM, any pair of (Z_T, Γ_T) univocally identifies one thermodynamic point on the $P-T$ diagram only, since Γ changes monotonically along Z isolines, as it can be seen in Figure 9a.

In the narrower thermodynamic region characterized by $Z_T \geq 0.6$, parameter Z_T is enough to identify a non-dimensional nozzle expansion. Indeed, as it can be seen in Figure 9a in this region the Γ gradient along Z isolines is limited. Thus, expansions at same Z_T exhibit very similar values of Γ_T. Moreover, within this region, Γ and Z gradients along isentropes are comparable, as shown in Figure 9b. This results in almost superimposed pressure ratio profiles along the nozzle axis, as detailed in 4.1.

However, it should be pointed out that, although different expansions sharing same $Z_T < 0.6$ exhibit different Γ_T values and Γ gradients, pressure ratio discrepancies at each nozzle section were found to be at most 5%.

The analysis and conclusions presented here are for fluid MM in its vapor close to the critical point region. It is worth investigating whether such findings hold in a wider thermodynamic region and for other organic fluids through *quasi-1D* calculation, as illustrated in the next section.

5. *Quasi-1D* isentropic expansions in non-ideal conditions

With the aim of giving a theoretical support to the presented experimental observations and in order to extend conclusions to a wider region of the thermodynamic plane and to other fluids, *quasi-1D* isentropic expansions were calculated for several P_T, T_T conditions sharing the same Z_T value. This was done for Z_T between 0.4 and 0.9 and for fluids MM, MDM, Toluene and Cyclopentane – fluids of interest in ORCs having high molecular complexity and weight and showing non-ideal behavior.

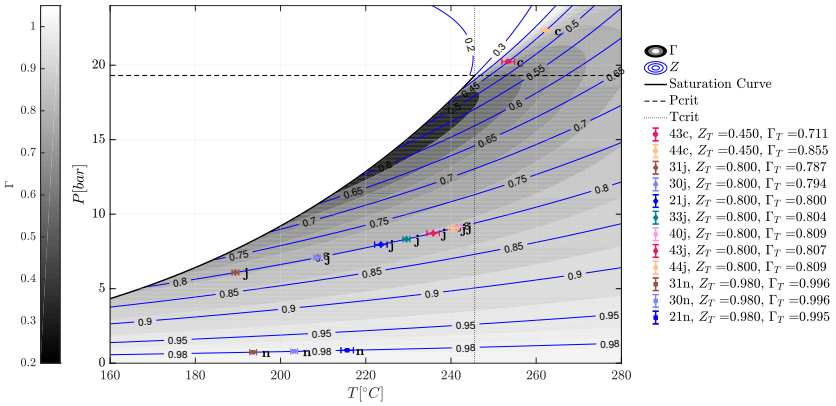

(a) *$P-T$ diagram with Γ contour and superimposed Z iso-lines reporting the total conditions of expansions sharing (c) $Z_T = 0.45$, (j) $Z_T = 0.80$ and (n) $Z_T = 0.98$.*

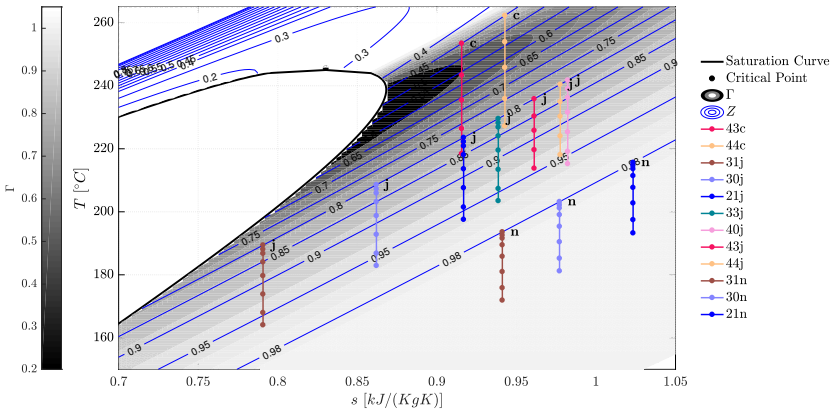

(b) *$T-s$ diagram with Γ contour and superimposed Z iso-lines reporting the expansions c, j and n.The dots correspond to the static temperatures computed from the static pressures measured.*

Figure 9

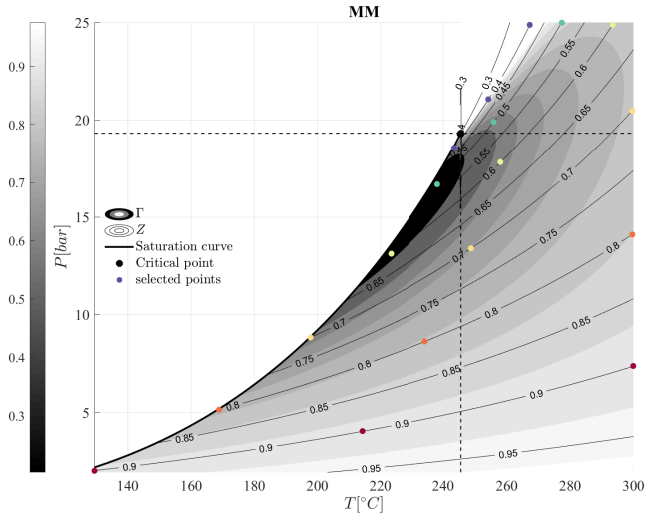

Figure 10: $P-T$ diagram with Z and Γ contours reporting total conditions selected at constant Z_T for *quasi-1D* calculation for fluid MM. Only three total conditions per Z_T are shown here for graphical clarity.

Total conditions at same Z_T were chosen so as to cover the largest possible area of the thermodynamic plane above critical conditions and between the saturation curve and the upper thermodynamic model limits (Figure 10).

For every total condition at each Z_T the area ratio A^*/A was plotted as a function of the pressure ratio in Figure 11. This is in analogy with experimental measurements, with the axial nozzle coordinate replaced by the generic A^*/A ratio.

In accordance with experimental results and as clearly seen in Figure 11, *quasi-1D* calculations show that in a fixed geometry the pressure ratio is larger for less ideal conditions. For example, considering sonic conditions, the pressure ratio can vary from about 0.71 at $Z_T = 0.4$ to 0.61 at $Z_T = 0.9$ for fluid MM, so by a non-negligible 16%. This is in line with experimental results reported in Section 3. Moreover, calculation confirm the good performance of Z_T as a similarity parameter for characterizing isentropic expansions for other fluids as well, with better performance as more ideal states are approached. To quantify

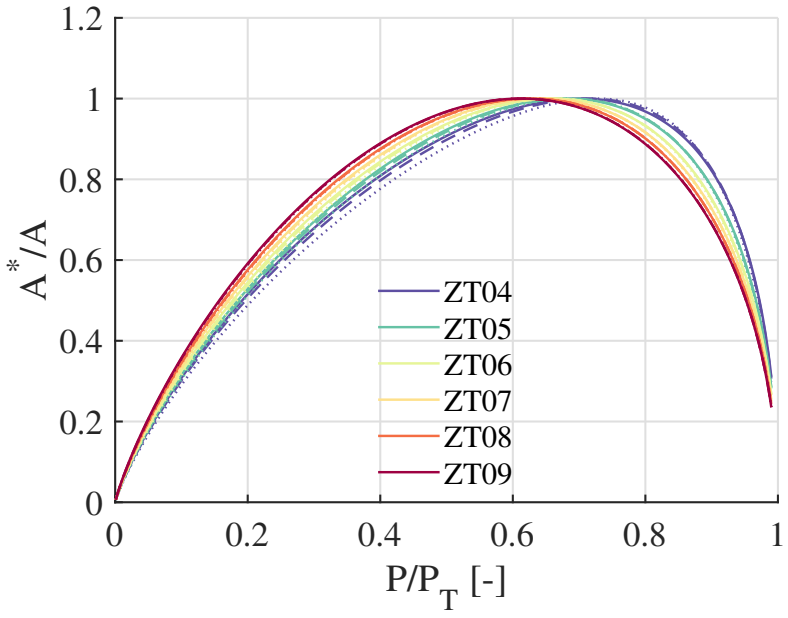

Figure 11: Area ratio as a function of pressure ratio at different total conditions for each Z_T (fluid MM). Only three total conditions per Z_T are shown here for graphical clarity. Each color corresponds to a different ZT value, while different line traits correspond to a different total condition.

A^*/A	0.8, sub	1	0.9, sup	0.7, sup
MM	0.1	3.5	6.5	7.5
MDM	0.2	1.1	1.6	1.6
Toluene	0.3	0.4	2.6	4.3
Cyclopentane	0.6	0.6	2.1	4.8

Table 2: Percentage pressure ratio variation $\Delta_{\Pi}^{Z_T}\%$ at $Z_T = 0.4$ and different total conditions, for different fluids

this, the percentage pressure ratio variation for expansions sharing same Z_T but having different total conditions $\Delta_{\Pi}^{Z_T}\%$ was calculated, as per Equation 3, at four values of area ratio for all fluids. The chosen A^*/A (0.8 subsonic, 1 sonic, 0.9 supersonic, 0.7 supersonic) correspond to Mach number values of interest in turbomachines, around 0.6, 1, 1.25 and 1.5 respectively. Table 2 reports the percentage pressure ratio variation for $Z_T = 0.4$, the worst performance case for parameter Z_T. $\Delta_{\Pi}^{Z_T}\%$ gets larger as the Mach number increases due to the lower pressure ratio at the denominator.

At the largest Mach number, the maximum variation of the pressure ratio at different total conditions and same $Z_T = 0.4$ is about 7.5%. At sonic and supersonic conditions all other fluids show lower values of $\Delta_{\Pi}^{Z_T}\%$ with respect to MM, confirming the satisfactory characterization of nozzle expansions by parameter Z_T.

6. Conclusion

This paper presented the results of an extensive experimental campaign conducted with fluid siloxane MM. The aim was the characterization of supersonic nozzle expansions in thermodynamic regions representative of ORC turbine applications. Analyzed expansions featured a wide range of total conditions, from

close to the critical point to almost ideal. It was possible to prove the non-ideal nature of the flow by measuring pressure ratios along the nozzle axis. Indeed, they proved to be dependent on total conditions, contrarily to what is expected for an ideal gas. In all axial locations where pressure measurements were available, the difference between the pressure ratio measured at the highest P_T and T_T ($Z_T \approx 0.40$) was higher by 10%-20% with respect to the one measured at the lowest P_T and T_T ($Z_T \approx 1$).

It was investigated whether one between parameters Z_T (Eq. 1) and Γ_T (Eq. 2) could be used to univocally identify a non-dimensional nozzle expansion. Two different analyses, one using sets of expansions sharing the same Z_T but featuring different P_T and T_T (Sec. 4.1), and the other using sets of expansions sharing the same Γ_T (Sec. 4.2), were carried out. It was concluded that, in the thermodynamic region explored with experiments between $Z_T = 0.60$ and $Z_T = 0.98$, parameter Z_T can be used as univocal identifier of non-dimensional MM nozzle expansions in a given geometry. Contrarily, in the region where $Z_T < 0.60$ another parameter is needed to univocally characterize a non-dimensional nozzle flow and a possible parameter can be Γ_T.

It was proven that Γ_T alone cannot be used to identify the level of non-ideality of a nozzle flow of siloxane MM. Indeed, the same values of Γ_T are found in thermodynamic regions featuring rarefied conditions, where non-ideal compressible effects are negligible, and also in regions close to the critical point where non-ideal effects play a major role.

The analysis, valid for fluid MM in its vapor phase close to the critical point region, was generalized to a broader thermodynamic region and to other fluids employed in ORCs by calculating *quasi-1D* isentropic expansions for several P_T, T_T conditions sharing the same Z_T value. This was done for Z_T between 0.4 and 0.9 and for fluids MM, MDM, Toluene and Cyclopentane. The maximum variation of the pressure ratio at different total conditions and same Z_T found was about 7.5%, confirming the satisfactory characterization of nozzle expansions by parameter Z_T also in regions showing $Z_T < 0.60$ and for a wider set of fluids.

Acknowledgements

The research is funded by the European Research Council under ERC Consolidator Grant 2013, project NSHOCK 617603.

Nomenclature

$21MM$ Name of a test run performed in the experimental campaign.

$21MMi$ Indicates a specific condition extracted from test 21MM. Each condition correspond to a steady state nozzle expansion.

Δ_Z Difference between two local compressibility factors computed at the same axial location but referring to different steady-state nozzle expansions. $\Delta_Z^{Z_T}$ refers to the difference computed between local Zs of two nozzle expansions sharing the same Z_T. $\Delta_Z^{\Gamma_T}$ refers to the difference computed between local Zs of two nozzle expansions sharing the same Γ_T.

Δ_Γ Difference between two values of local Γ computed at the same axial location but referring to different steady-state nozzle expansions.$\Delta_\Gamma^{Z_T}$ refers to the difference computed between local Γs of two nozzle expansions sharing the same Z_T. $\Delta_\Gamma^{\Gamma_T}$ refers to the difference computed between local Γs of two nozzle expansions sharing the same Γ_T.

$\Delta_\Pi\%$ Difference between two pressure ratios measured at the same axial location but referring to different steady-state nozzle expansions expressed as a percentage referred to the minumum between the two pressure ratios subtracted.

Δ_Π Difference between two pressure ratios measured at the same axial location but referring to different steady-state nozzle expansions. $\Delta_\Pi^{Z_T}$ refers to the difference computed between two nozzle expansions sharing the same Z_T. $\Delta_\Pi^{\Gamma_T}$ refers to the difference computed between two nozzle expansions sharing the same Γ_T.

Γ Fundamental derivative of gasdynamic

$\Pi = P/P_T$ Pressure ratio

ρ Density $[kg/m^3]$

A^*/A Ratio between the area at sonic conditions and the local area of a nozzle.

c Speed of sound $[m/s]$

H Throat semi-height $[mm]$

M Mach number

$M1.6$ Name of the nozzle tested

P Pressure $[bar]]$

R Gas constant $[J/kgK]$

r_t Ratio between the radius of the circular arc shaping the nozzle throat and the throat semi-height

T Temperature $[°C]$

v Specific Volume $[m^3/kg]$

x/H Non-dimensional axial coordinate

Z Compressibility factor

s Entropy $[kJ/kgK]$

Subscript T Total quantities

References

[1] P. Colonna, E. Casati, C. Trapp, T. Mathijssen, J. Larjola, T. Turunen-Saaresti, A. Uusitalo, Organic rankine cycle power systems: From the concept to current technology, application, and an outlook to the future, Journal of Engineering for Gas Turbine and Power 137 (2015) 100801–100801–19 (2015).

[2] E. Macchi, M. Astolfi, Organic Rankine Cycle (ORC) Power Systems. Technologies and applications, Woodhead Publishing Series in Energy, New York, 2017 (2017).

[3] T. Tartiere, M. Astolfi, A world overview of the organic rankine cycle market, Energy Procedia 129 (2017) 2 – 9, 4th International Seminar on ORC Power SystemsSeptember 13-15th 2017POLITECNICO DI MILANOBOVISA CAMPUSMILANO, ITALY (2017). doi:https://doi.org/10.1016/j.egypro.2017.09.159.
URL http://www.sciencedirect.com/science/article/pii/S1876610217340286

[4] A. Spinelli, G. Cammi, S. Gallarini, M. Zocca, F. Cozzi, P. Gaetani, V. Dossena, A. Guardone, Experimental evidence of non-ideal compressible effects in expanding flow of a high molecular complexity vapor, Experiments in Fluids 59 (8) (2018) 126 (Jul 2018). doi:10.1007/s00348-018-2578-0.
URL https://doi.org/10.1007/s00348-018-2578-0

[5] A. Spinelli, G. Cammi, C. C. Conti, S. Gallarini, M. Zocca, F. Cozzi, P. Gaetani, V. Dossena, A. Guardone, Experimental observation and thermodynamic modeling of non-ideal expanding flows of siloxane mdm vapor for orc applications, Energy 168 (2019) 285 – 294 (2019). doi:https://doi.org/10.1016/j.energy.2018.11.071.

[6] P. Colonna, J. Harinck, S. Rebay, A. Guardone, Real-gas effects in organic rankine cycle turbine nozzles, Journal of Propulsion and Power 24 (2008) 282–294 (2008).

[7] S. Vitale, G. Gori, M. Pini, A. Guardone, T. D. Economon, F. Palacios, J. J. Alonso, P. Colonna, Extension of the SU2 open source CFD code to the simulation of turbulent flows of fuids modelled with complex thermophysical laws, in: 22nd AIAA Computational Fluid Dynamics Conference, no. AIAA Paper 2760, 2015 (2015).

[8] M. Pini, G. Persico, D. Pasquale, S. Rebay, Adjoint method for shape optimization in real-gas flow applications, Journal of Engineering for Gas Turbines and Power 137 (3) (2015).

[9] S. Vitale, T. A. Albring, M. Pini, N. R. Gauger, P. Colonna, Fully turbulent discrete adjoint solver for non-ideal compressible flow applications, Journal of the Global Power and Propulsion Society 1 (2018) 252 – 270 (2018). doi:10.22261/JGPPS.Z1FVOI.
URL https://journal.gpps.global/a/Z1FVOI/

[10] G. Persico, M. Pini, V. Dossena, P. Gaetani, Aerodynamics of centrifugal turbine cascades, ASME J. Eng. Gas Turb. Power 137 (112602) (2015) 1–11 (2015).

[11] G. Gori, M. Zocca, G. Cammi, A. Spinelli, P. Congedo, A. Guardone, Accuracy assessment of the non-ideal computational fluid dynamics model for siloxane mdm from the open-source su2 suite, European Journal of Mechanics - B/Fluids 79 (2020) 109–120 (2020). doi:10.1016/j.euromechflu.2019.08.014.

[12] R. Span, W. Wagner, Equations of state for technical applications. II. Results for nonpolar fluids, International Journal of Thermophysics 24 (1) (2003) 41–109 (January 2003).

[13] M. Thol, F. Dubberke, E. Baumhögger, J. Vrabec, R. Span, Speed of sound measurements and fundamental equations of state for octamethyltrisiloxane and decamethyltetrasiloxane, Journal of Chemical and Engineering Data 62 (9) (2017) 2633–2648 (2017). doi:10.1021/acs.jced.7b00092.
URL https://www.scopus.com/inward/record.uri?eid=2-s2.0-85029502909&doi=10.1021%2facs.jced.7b00092&partnerID=40&md5=49f3275dba830db9f761640c0e20c61d

[14] F. J. Dura Galiana, A. P. S. Wheeler, J. Ong, A study of trailing-edge losses in organic rankine cycle turbines, Journal of Turbomachinery 138 (12 2016).

[15] M. Robertson, P. Newton, T. Chen, A. Costall, R. F. Martinez-Botas, Experimental and numerical study of supersonic non-ideal flows for organic rankine cycle applications, Journal of Engineering for Gas Turbines and Power (03 2020). doi:10.1115/1.4046758.

[16] T. Mathijssen, M. Gallo, E. Casati, N. R. Nannan, C. Zamfirescu, A. Guardone, P. Colonna, The flexible asymmetric shock tube (FAST): a ludwieg tube facility for wave propagation measurements in high-temperature vapours of organic fluids, Experiments in Fluids 56 (10) (2015) 195 (Oct 2015). doi:10.1007/s00348-015-2060-1.
URL https://doi.org/10.1007/s00348-015-2060-1

[17] A. J. Head, C. D. Servi, E. Casati, M. Pini, P. Colonna, Preliminary design of the ORCHID: a facility for studying non-ideal compressible fluid dynamics and testing ORC expanders, Proceedings of ASME Turbo Expo (2016).

[18] F. Reinker, E. Y. Kenig, M. Passmann, S. aus der Wiesche, Closed loop organic wind tunnel (CLOWT): Design, components and control system, Energy Procedia 129 (2017) 200 – 207, 4th International Seminar on ORC Power SystemsSeptember 13-15th 2017 (2017). doi:https://doi.org/10.1016/j.egypro.2017.09.158.
URL http://www.sciencedirect.com/science/article/pii/S1876610217340274

[19] A. Spinelli, M. Pini, V. Dossena, P. Gaetani, F. Casella, Design, simulation and construction of a test rig for organic vapors, ASME Journal of Engineering for Gas Turbine and Power 135 (2013) 042304–042304–10 (2013).

[20] M. Pini, A. Spinelli, V. Dossena, P. Gaetani, F. Casella, Dynamic simulation of a test rig for organic vapours, Proceedings of ASME 5th International Conference on Energy Sustainability (2011) 1977–1988 (2011).

[21] A. Guardone, A. Spinelli, V. Dossena, Influence of molecular complexity

on nozzle design for an organic vapor wind tunnel, Journal of Engineering for Gas Turbines and Power 135 (april 2013).

[22] P. A. Thompson, A fundamental derivative in gasdynamics, Physics of Fluids (1958-1988) 14 (9) (1971) 1843–1849 (1971).

[23] D. Vimercati, G. Gori, A. Guardone, Non-ideal oblique shock waves, Journal of Fluid Mechanics 847 (2018) 266285 (2018). doi:10.1017/jfm.2018.328.